

# Journal of Materials Chemistry A

Accepted Manuscript



This is an *Accepted Manuscript*, which has been through the Royal Society of Chemistry peer review process and has been accepted for publication.

*Accepted Manuscripts* are published online shortly after acceptance, before technical editing, formatting and proof reading. Using this free service, authors can make their results available to the community, in citable form, before we publish the edited article. We will replace this *Accepted Manuscript* with the edited and formatted *Advance Article* as soon as it is available.

You can find more information about *Accepted Manuscripts* in the [Information for Authors](#).

Please note that technical editing may introduce minor changes to the text and/or graphics, which may alter content. The journal's standard [Terms & Conditions](#) and the [Ethical guidelines](#) still apply. In no event shall the Royal Society of Chemistry be held responsible for any errors or omissions in this *Accepted Manuscript* or any consequences arising from the use of any information it contains.

Cite this: DOI: 10.1039/c0xx00000x

ARTICLE TYPE

www.rsc.org/xxxxxx

# Non-Ultraviolet Photocatalytic Kinetics on NaYF<sub>4</sub>:Yb,Tm@TiO<sub>2</sub>/Ag Core@Comby Shell Nanostructures

Yongmei Ma, Honglin Liu,\* Zhenzhen Han, Liangbao Yang,\* and Jinhui Liu

Received (in XXX, XXX) Xth XXXXXXXXXX 20XX, Accepted Xth XXXXXXXXXX 20XX

DOI: 10.1039/b000000x

An effective near-infrared (NIR) active photocatalyst, NaYF<sub>4</sub>:Yb,Tm@TiO<sub>2</sub>/Ag (UC@TiO<sub>2</sub>/Ag) core@comby shell composite was synthesized by a simple three-step hydrothermal process. Under full-spectrum lights of Xe lamp in UV-Vis absorbance experiments, about 96% of R6G dyes in solution were degraded by UC@TiO<sub>2</sub>/Ag in 120 minutes, while only about 64% of dyes were degraded by pure TiO<sub>2</sub> at the same conditions. Under UV-filtered Xe lamp, about 35% of dyes were degraded by UC@TiO<sub>2</sub>/Ag in 120 minutes; interestingly only about 8% of dyes were degraded by pure TiO<sub>2</sub>. Under irradiation of 785 nm laser in surface enhanced Raman scattering (SERS) experiments, the photodegradation rate constants were 0.02612 s<sup>-1</sup> for UC@TiO<sub>2</sub>/Ag and 0.00046 s<sup>-1</sup> for TiO<sub>2</sub>/Ag, indicating an improvement of nearly 58 times. After deducting the photobleaching effect, those for UC@TiO<sub>2</sub>/Ag under 633 and 532 nm lasers are 0.00715 s<sup>-1</sup> and 0.00565 s<sup>-1</sup>, respectively, revealing a sharp decrease under irradiation of shorter wavelengths. Electron spin resonance (ESR) analysis revealed that the presence of UC in this photocatalytic system certainly induced the increase of the ·OH free radicals with the NIR irradiation, i.e. the UC core converts NIR light into ultraviolet (UV) light and initiates excellent photocatalytic activity of the TiO<sub>2</sub>/Ag comby shell. Furthermore, the decorating of Ag nanoparticles not only enhances the photocatalytic ability, but also provides structural basis for monitoring photocatalytic kinetics by SERS technique. By virtue of monochrome laser lines, SERS analysis provides the direct evidence to prove the capability of UC-initiated non-UV photocatalysis and the improvement of the utilization of non-UV lights on TiO<sub>2</sub>. The results revealed that this new photocatalytic platform can efficiently utilize different bands of the solar spectrum and also find new applications in SERS fields.

## Introduction

There has been a world-wide focus on the photocatalytic degradation of pollutants by the use of novel nanomaterials. Titanium dioxide (TiO<sub>2</sub>), the most promising photocatalyst, has been widely studied on degrading inorganic or organic pollutants because of its strong oxidizing power under ultraviolet (UV) light, extraordinary chemical stability, biocompatible features and environmental friendliness.<sup>1, 2</sup> However, it requires UV light activation source due to its large band gap of ca. 3.2 eV (for the crystalline anatase phase).<sup>3</sup> As is well-known, the percentage of UV light in the solar spectrum is only ca. 5%, whereas the visible and NIR lights occupy ca. 49% and ca. 46%, respectively.<sup>4</sup> The photocatalytic efficiency of pure TiO<sub>2</sub> in the environmental remediation has been restrained because of the low-usage of sunlight. To solve this problem, many efforts have been devoted to extending the absorption of TiO<sub>2</sub> to the visible or even NIR region for better use of solar energy.<sup>5-7</sup> Numerous methods have been reported to adjust the band gap of TiO<sub>2</sub> toward visible light energies through introducing noble metals and nonmetallic

elements, cationic substitutions, or anionic doping.<sup>8-12</sup> Unfortunately, the overall catalytic capability of TiO<sub>2</sub> decreases when its absorption was adjusted to visible and NIR regions by those modification methods.<sup>13, 14</sup> To date, it remains a great challenge to extend the absorption of TiO<sub>2</sub> to the visible and NIR regions and meanwhile keep its catalytic capability. An attractive and promising strategy is to couple the photocatalytic center with semiconductor materials that can result in non-linear optical processes, transfer photoexcited electrons to the photocatalytic agent, and then initiate and enhance the photoreactions.<sup>15, 16</sup> Particularly, the upconversion (UC) emission materials can convert NIR light into visible or UV light, i.e. two or more low-energy pump photons can be converted to a higher-energy output photon.<sup>17, 18</sup> In addition, UC materials show many exciting features including a sharp emission bandwidth, large anti-Stokes shifts (up to 500 nm), high photostability, tunable emission, and low cytotoxicity. These features lead to potential applications in lasers, next-generation lighting, infrared quantum counters, and biological macromolecular systems. UC materials have been used in a variety of assay formats ranging from bio-detection to cancer therapy.<sup>19, 20</sup> As UC materials can efficiently

convert NIR light into UV emissions, it is very interesting to integrate the UC materials with UV-active photocatalysts to harvest solar energy in a broader spectral range by the use of UC materials as a frequency conversion element for photocatalysts. If such a hybrid structure was used as a new type of photocatalysts to work under NIR irradiation, the utilization efficiency of sunlight might be greatly improved. Most recently, the researchers have tried to synthesize  $\text{YF}_3:\text{Yb}^{3+},\text{Tm}^{3+}/\text{TiO}_2$  core-shell structures for sunlight photocatalytic investigations.<sup>21, 22</sup> However, the  $\text{YF}_3$  is a low efficient host for upconversion luminescence, which limits the further investigation on its catalytic performance and other potential applications. And these reports didn't present solid evidences to convincingly prove the UC-related improvement on photocatalytic efficiency of  $\text{TiO}_2$  under the sunlight. Another bottleneck in developing this kind of photocatalytic strategies is the difficulty in monitoring early events of the catalytic reaction kinetics.

To date, surface-enhanced Raman spectroscopy (SERS) has become one of the most widely used spectroscopic tools for the identification and detection of inorganic and organic dye pollutions, with the integration of the single-molecule level sensitivity and individually discernable fingerprints from molecular vibrations.<sup>23-27</sup> We speculate that the SERS technique has particular advantages in providing information on the function of UC materials in photocatalytic reaction, the catalytic reaction kinetics, and the underlying mechanism of a new type of non-UV photocatalytic materials. In fact, the coupling of UC materials with noble metal nanoparticles such as Ag and Au has been developed as a valuable strategy to enhance their luminescence.<sup>28, 29</sup> This enhancement can be at least partly attributed to surface plasmon-coupled emission, which can increase the radiative decay rate and emission efficiency.<sup>30</sup> More importantly, the existence of noble metal nanoparticles can provide the feasibility of SERS analysis. Compared to UV-vis spectroscopy, SERS technique highlights the superiorities of ultra-sensitivity, single wavelength laser, and high time-resolution as a photocatalytic testing tool.<sup>31</sup>

Herein, we synthesized a nanostructure hybrid ( $\text{UC@TiO}_2/\text{Ag}$ ) consisting of a comby  $\text{TiO}_2/\text{Ag}$  shell and a hexagonal  $\text{NaYF}_4:\text{Yb},\text{Tm}$  microcrystal core as non-UV photocatalysis. Our procedure for material fabrication is easily operated, low cost and scalable. We tried to improve the utilization efficiency of non-UV lights on  $\text{TiO}_2$  and prove the function of UC materials in the non-UV photocatalytic reaction. In this system, Ag nanoparticles in  $\text{UC@TiO}_2/\text{Ag}$  hybrid act as both the luminescence enhancers and the SERS-active substrates. More importantly, both the UV-filtered Xe lamp and monochrome laser lines on SERS apparatus were used to investigate the photocatalytic activities of this core@comby shell nanocomposites; while the catalytic reaction kinetics could be facilely monitored by SERS technique. We provided direct evidence to prove the capability of UC-initiated non-UV photocatalysis and the improvement of the utilization of non-UV lights on  $\text{TiO}_2$ . The results revealed that this new photocatalytic platform can efficiently utilize different bands of the solar spectrum and also find new applications in SERS fields. The core-comby shell hybrid structures also provide a new direction for the synthesis of novel photocatalysts, and promise many attractive potential applications in optics, plasmonics, and

catalysis fields.

## 60 Experimental section

### Chemicals and materials

Silver nitrate ( $\text{AgNO}_3$ ), sodium citrate, para-aminothiophenol (PATP), NaF,  $\text{TmCl}_3$ ,  $\text{YbCl}_3 \cdot 6\text{H}_2\text{O}$ ,  $\text{YCl}_3 \cdot 6\text{H}_2\text{O}$ , Ethylene Diamine Tetraacetic (EDTA), Titanium n-butoxide ( $\text{Ti}(\text{OBU})_4$ ), Alcohol, Crystal violet (CV), and Rhodamine 6G (R6G) were purchased from Shanghai Reagent Co.; 5,5-Dimethyl-1-pyrroline N-oxide (DMPO) was purchased from Aladdin chemical Co., and all of these chemicals were A.R. grade and used without further purification. The solutions were prepared with distilled water without further pH regulation, and all experiments were carried out under room temperature (25 °C) in water system without any buffer.

### Synthesis of upconversion materials

A hydrothermal method<sup>32</sup> was simply modified to synthesize UC microcrystals by using trisodium citrate as a capping agent. An aqueous solution of  $\text{YCl}_3 \cdot 6\text{H}_2\text{O}$ ,  $\text{YbCl}_3 \cdot 6\text{H}_2\text{O}$ , and  $\text{TmCl}_3$  (lanthanide ion molar ratio, Y/Yb/Tm=79.5:20:0.5) was mixed with an aqueous solution of 1% trisodium citrate under vigorous stirring, producing a white complex. Then 1.2 mol/L NaF aqueous solution (25 mL) was added into the complex solution, which was stirred for 1 h. The newly-formed complex precursor solution was then transferred into a 60 ml autoclave and heated at 180 °C for 3 h. The UC microcrystals were then separated via centrifugation and rinsed several times with ultrapure water.

### 85 Preparation of $\text{TiO}_2$ decorated $\text{NaYF}_4:\text{Yb},\text{Tm}$ ( $\text{UC@TiO}_2$ for short)

Titanium n-butoxide ( $\text{Ti}(\text{OBU})_4$ ) was employed as the Ti source because the hydrolysis rate of  $\text{Ti}(\text{OBU})_4$  was ca. 150 times slower than that of tetraethyl titanate,  $\text{Ti}(\text{OEt})_4$ .<sup>4</sup> A typical procedure for coating titania onto UC microcrystals has been described as follows: UC microcrystals were dispersed in ethanol, then  $\text{Ti}(\text{OBU})_4$  was added into the solution above. This newly-formed complex precursor solution was transferred into a 60 ml autoclave which contains 5 mL ultrapure water and heated at 180 °C for 20 h. The resulting product was collected by centrifugation, washed several times with distilled water and ethanol, respectively, and then dried at 60 °C in drying oven.

### Preparation of Ag nanoparticles decorated $\text{UC@TiO}_2$ ( $\text{UC@TiO}_2/\text{Ag}$ for short)

The decorating of Ag nanoparticles onto the  $\text{UC@TiO}_2$  was performed by the use of trisodium citrate as both the coupling agent and the reductant. The dried  $\text{UC@TiO}_2$  powders were dispersed in ultrapure water, and 0.1mol/L  $\text{AgNO}_3$  (0.25 mL) was added into the solution, and then the mixture solution was stirred and heated to 100 °C. Then 1% trisodium citrate (1 mL) was added into the boiling solution, keep the temperature of the mixed solution for 1 hour. The obtained products were centrifugally precipitated, and rinsed several times with ultrapure water.

### Photocatalytic experiments

The photocatalytic activities of the  $\text{UC@TiO}_2/\text{Ag}$  were evaluated by the degradation of R6G under the irradiation of a Xe lamp (set

at 50 W). In a typical process, a certain amount of the UC@TiO<sub>2</sub>/Ag particles was dispersed into 50 mL 1×10<sup>-5</sup> mol/L R6G solution in a quartz tube. To determine the real concentration of R6G in photocatalytic degradation, the solution was then stirred for 12 h in dark to reach an adsorption-desorption equilibrium between the nanoparticles and the solution. Subsequently, the beaker was exposed to irradiation of the Xe lamp, 3 mL of R6G aqueous solution was intermittently collected at given time intervals for centrifugation, the filtrates were measured the absorbance by UV-vis spectroscopy and the remainder composites was measured the intensity by SERS. To further verify the universality of UC@TiO<sub>2</sub>/Ag, a resonant dye molecule CV, also a widely-used SERS reporter, was used to investigate the catalytic reaction kinetics by SERS. A certain amount of the UC@TiO<sub>2</sub>/Ag particles was decorated in capillary tube, 15 μL 1×10<sup>-5</sup> M R6G solution was imported into the capillary tube, and then monitoring the kinetics using SERS after 2 h in dark. A time-course SERS mapping of the catalytic reaction kinetics of UC@TiO<sub>2</sub>/Ag was performed under continuous exposure to a 785 nm laser.

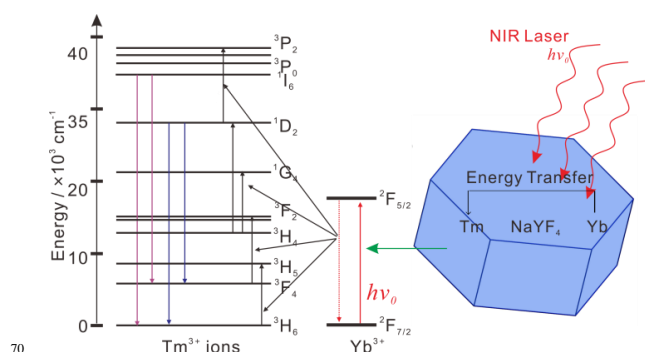
### Apparatus

The scanning electron microscopy (SEM) images were taken by a Sirion 200 field-emission scanning electron microscope. X-Ray scattering patterns were conducted by analyzing the powder samples on a Philips X-Pert Pro X-ray diffractometer (XRD) with Cu Kα radiation. Transmission electron microscopy (TEM) images were recorded by a JEOL 2010 high resolution transmission electron microscope, equipped with X-ray energy dispersive spectroscopy (EDS) capabilities, operated at an acceleration voltage of 200 kV. Upconversion luminescence spectra were recorded by using a fluorescence spectrophotometer under the excitation of a 980 nm laser. SERS spectra were carried out on a LabRAM HR800 confocal microscope Raman system (Horiba Jobin Yvon) by the use of three different monochrome laser lines – an Ar ion laser of 785 nm, a He-Ne laser of 633 nm, and a Nd:YAG laser of 532 nm. The lasers were focused by a LWD 50×0.5 NA objective lens and the laser spots had a diameter of about 1 μm. The laser powers on sample location were all adjusted to approximately 0.5 mW. The grating was 600 g/mm. The exposure time for each spectrum was 1 s and the increment time in time-course SERS mapping was 2 s. The data process and baseline correction were performed using the LabSpec V5.58.25 software. Electron spin resonance (ESR) measurement was conducted on a Bruker X-band (9.4 GHz) EMS plus 10/12 spectrometer. 1 mg different photocatalysts was dispersed in water (1 ml), then 20 μl DMPO was added into the solution respectively, and the solution was transferred to an EPR tube. A cylindrical resonator (ER4119hs TE011) was used for data collection. A Xe lamp (100 W) was used as the light source. All the ESR data were collected at the High Magnetic Field Laboratory (Hefei City), Chinese Academy of Sciences.

### Results and discussion

On the theory of design, the UC cores can efficiently convert NIR excitation into UV emissions, we speculate that the incorporation of UC cores into UV-active photocatalysts might provide a new way to improve the utilization efficiency of sunlight. As shown in

scheme 1, under the NIR excitation of 785 nm, the Yb<sup>3+</sup> ions act as sensitizers and are the primary absorbers of the NIR excitation. Yb<sup>3+</sup> then transfer the energy absorbed from the NIR excitation to Tm<sup>3+</sup>, Tm<sup>3+</sup> ions are excited by the Yb<sup>3+</sup> → Tm<sup>3+</sup> energy transfer, and then three successive energy transfers from Yb<sup>3+</sup> to Tm<sup>3+</sup> populate the <sup>3</sup>H<sub>5</sub>, <sup>3</sup>F<sub>2</sub>, and <sup>1</sup>G<sub>4</sub> levels. The sequential energy absorption from two excited Yb<sup>3+</sup> ions promotes Tm<sup>3+</sup> to <sup>1</sup>D<sub>2</sub> and <sup>3</sup>P<sub>2</sub>. Finally, the excited Tm<sup>3+</sup> ions fall to lower energy levels. UV emission peaks centered at 349 and 362 nm corresponding to the transitions of Tm ions: <sup>1</sup>I<sub>6</sub> → <sup>3</sup>F<sub>4</sub> and <sup>1</sup>D<sub>2</sub> → <sup>3</sup>H<sub>6</sub> could be observed under the 785 nm excitation lasers. Two blue emission peaks centered at 450 and 474 nm are assigned to <sup>1</sup>D<sub>2</sub> → <sup>3</sup>F<sub>4</sub> and <sup>1</sup>G<sub>4</sub> → <sup>3</sup>H<sub>6</sub> transitions of Tm<sup>3+</sup> ions, respectively.<sup>33</sup>



Scheme 1 Illustration of the relevant processes of energy transfer in UC cores.

In the aspect of experiments, the hexagonal flake of UC microcrystals with uniform size and shape were successfully synthesized by a simple hydrothermal method. Their average side length was ca. 400 nm which was clearly revealed in the TEM image (the inset of Fig. S1). NaYF<sub>4</sub> has been widely recognized as one of the most efficient hosts for upconversion rare-earth (RE) ions sensitized by Yb<sup>3+</sup>, and high-efficient multicolor UC in UV and blue luminescences. It is worth mentioning that strong UV light is obtained in UC microcrystals upon NIR excitation, which is especially useful for realizing the NIR-driven photocatalytic activity of UC@TiO<sub>2</sub>/Ag that will be investigated in the following section. Here, Ti(OBu)<sub>4</sub> was employed as the Ti source and the thickness of TiO<sub>2</sub> can be facilely controlled by adjusting the amount of Ti(OBu)<sub>4</sub> as shown in Fig. S2. But a thick shell of TiO<sub>2</sub> greatly shielded the upconversion efficiency of UC (data not shown), we found that a shell of about 50-100 nm could ensure an acceptable upconversion efficiency of UC cores and keep a high photocatalytic activity of TiO<sub>2</sub>. After coating UC microcrystals with titania, a simple procedure was developed to decorate Ag nanoparticles on the surface of this microcrystal. As shown in Fig. 1A-D, the titania and Ag nanoparticles were successfully decorated on the surface of UC microcrystals, and the UV emission peaks of UC@TiO<sub>2</sub>/Ag centered at 349 and 362 nm (inset in Fig. 1B). HRTEM image showed that the lattice fringe with the spacing of about 0.35 nm corresponds to the (101) plane of anatase titania and the spacing of 0.24 nm corresponds to the (111) plane of the Ag nanoparticles. Moreover, the HRTEM at high angle annular dark field (HAADF) further evidenced that all elements of Ag, Ti, Tm and Yb distributed throughout the entire particle (Fig. 1E-H). The elemental mapping profiles also

provided exclusive evidence of the presence of the titania and Ag, their distribution patterns, and the comby shell of TiO<sub>2</sub>/Ag decorated on UC microcrystals.

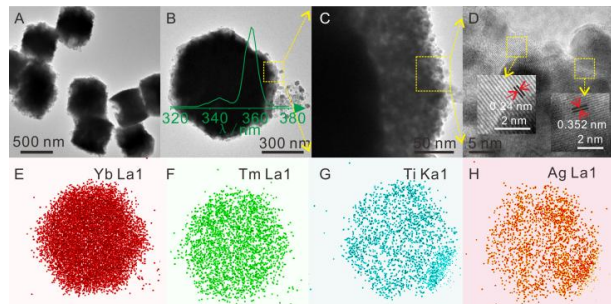


Fig. 1 (A-C) TEM images of UC@TiO<sub>2</sub>/Ag particles with different magnification (inset in B: the corresponding emission spectrum of UC@TiO<sub>2</sub>/Ag). (D) HRTEM image of enlarged detail of the TiO<sub>2</sub>/Ag comby shell. (E-H) EDX elemental mapping of a single particle of UC@TiO<sub>2</sub>/Ag, including Yb La1, Tm La1, Ti Ka1 and Ag La1.

such as Au or Ag NPs, the broad absorption of noble metals can increase the power of the excitation by local field enhancement, resulted in the increase of excited Yb<sup>3+</sup> ions, and more energy was transferred from excited Yb<sup>3+</sup> to Tm<sup>3+</sup>.<sup>34</sup>

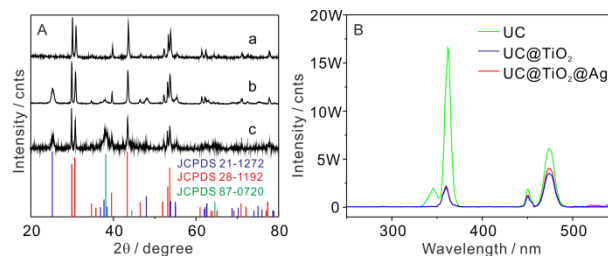


Fig. 2 (A) XRD patterns of UC microcrystals (a), UC@TiO<sub>2</sub> (b) and UC@TiO<sub>2</sub>@Ag (c), and standard XRD patterns of NaYF<sub>4</sub> (JCPDS 28-1192), anatase-phase TiO<sub>2</sub> (21-1272) and Ag (87-0702). (B) PL spectra of UC microcrystals (green line), UC@TiO<sub>2</sub> (blue line) and UC@TiO<sub>2</sub>@Ag (red line) under the NIR excitation.

The XRD pattern of UC microcrystals (curve a in Fig. 2A) is in good agreement with the standard values for the hexagonal-phase NaYF<sub>4</sub> crystals (JCPDS files No.28-1192). Hexagonal NaYF<sub>4</sub> is a more efficient host for upconversion luminescence than cubic NaYF<sub>4</sub> and YF<sub>3</sub>. The XRD patterns of TiO<sub>2</sub>-decorated UC microcrystals (curve b in Fig. 2A) evidenced the successful decorating of anatase-phase TiO<sub>2</sub> on UC microcrystals. The new peaks at 2θ = 38.0, 44.2, 64.4, and 77.3 in curve c in Fig. 2A are consistent with the face Ag (JCPDS files No.87-0720). Fig. 2B presents the PL spectra of UC microcrystals (green line), UC@TiO<sub>2</sub> (blue line) and UC@TiO<sub>2</sub>@Ag (red line) under the NIR excitation. The intensities of 349, 362, 450, and 474 nm peaks originated from UC microcrystals are 19000, 165000, 19000, and 60000 cnts, respectively. Interestingly, the coating of anatase-phase TiO<sub>2</sub> resulted in notable alterations of PL spectrum. Compared the PL spectrum of UC@TiO<sub>2</sub> with UC, the emission peak at 349 nm nearly disappeared and the intensities of 362, 450, and 474 nm peaks decreased to ca. 16150, 10870, and 35300 cnts, respectively. By comparison, the emission peaks at 450 and 474 nm decreased by about 42%. This decrease could be attributed to the shielding effect of the existing TiO<sub>2</sub> comby shell on light conversion of UC microcrystals. More interestingly, the 349 nm peak disappears and the intensity of 362 nm peak decreased by about 90% after coating TiO<sub>2</sub>. The relative change of each peak intensity cannot be simply explained only by the shielding effect, the major reason of this phenomenon should be ascribed to the shell absorbance, i.e. a crystallized TiO<sub>2</sub> comby shell can efficiently absorb UV lights (~350 nm) emitted from UC cores upon NIR irradiation. In more detail, two excited state levels, <sup>1</sup>I<sub>6</sub> and <sup>1</sup>D<sub>2</sub>, match with the band gap of TiO<sub>2</sub> (Scheme 1).<sup>4</sup> And the energy migration to TiO<sub>2</sub> made a prerequisite to realize NIR responsive photocatalysis of broadband TiO<sub>2</sub>. It's worth noting that the coating of Ag on UC@TiO<sub>2</sub> resulted in enhancement of PL spectrum. The intensities of 362, 450, and 474 nm peaks originated from UC microcrystals are 17670, 12500 and 40620 cnts, respectively. The intensity of UC@TiO<sub>2</sub>@Ag is about 1.15 folds that of UC@TiO<sub>2</sub>. We can deduce that Ag can penetrate the appropriate thickness of comby TiO<sub>2</sub> effect on the upconversion efficiency of UC materials. In the presence of noble metals NPs,

Firstly, full-spectrum Xe lamp was used in this section for photocatalytic degradation. A dye molecule, Rhodamine 6G (R6G), as a model pollutant was used to investigate the photocatalytic activity of UC@TiO<sub>2</sub>/Ag hybrid materials under a 50W Xe lamp. A certain amount of UC@TiO<sub>2</sub>/Ag particles was dispersed into 1 × 10<sup>-5</sup> M R6G (50 mL) in a quartz tube. For obtaining the accurate concentration of R6G in photocatalytic degradation, the solution was first stirred for 12 h in dark to reach an adsorption-desorption equilibrium between the nanoparticles and the solution. Upon Xe lamp irradiation for a designated time, 3 mL of R6G aqueous solution was taken out and centrifuged, then the supernatant was used for measuring the absorbance of UV-vis spectroscopy and the remainder composites were used for SERS measurements. Fig. 3A showed the absorbance spectra of R6G catalyzed by UC@TiO<sub>2</sub>/Ag hybrid materials under Xe lamp irradiation as a function of the irradiation time. The absorption intensity of R6G at 520 nm decreased gradually with increasing irradiation time, indicating the degradation of R6G upon the Xe lamp irradiation. The photocatalytic activity of UC@TiO<sub>2</sub>/Ag could be evaluated by comparing the supernatant concentration at each exposure time to that at time ZERO.

To examine the function of UC cores in the photocatalytic process, a series of parallel experiments in the absence or presence of each photocatalyst were performed in the following. Fig. 3B plotted time-dependent curves of C<sub>t</sub>/C<sub>0</sub> ratio, an indicator of the degradation degree. C<sub>0</sub> was the original concentration of R6G at time ZERO and C<sub>t</sub> was the supernatant concentration of R6G after the sample was irradiated with a Xe lamp for a time t. C<sub>t</sub> was obtained by comparing the 520 nm absorbance of R6G solution with that of standard R6G solution. Under irradiation of full-spectrum Xe lamp, (i) almost no degradation of R6G occurred in the absence of any photocatalyst. It also revealed that only a very small amount of R6G was adsorbed on particle surfaces in the dark reaction so that these adsorptions were almost negligible for calculating the degradation ratio of photocatalytic reaction. (ii) In the presence of TiO<sub>2</sub>, ca. 64% of R6G in solution was degraded after 2 h. (iii) In the presence of UC@TiO<sub>2</sub>, nearly 93% of R6G was degraded after 2 h. (iv) In the presence of UC@TiO<sub>2</sub>/Ag hybrid materials, the degradation ratio of R6G

increased continuously with increasing the irradiation time and reached about 96% after 2 h irradiation.

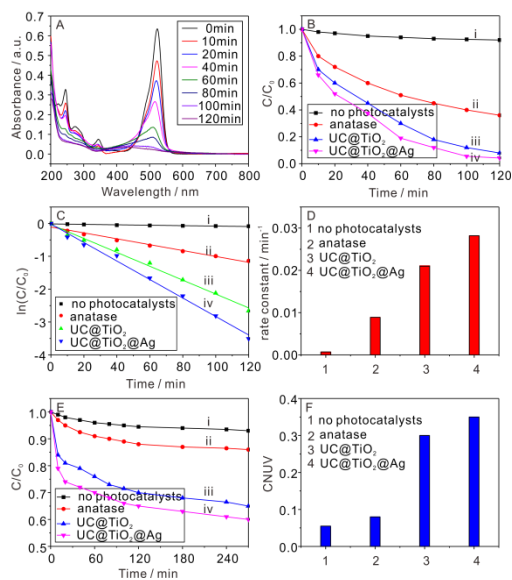


Fig. 3. (A) Time-course UV-Vis absorbance spectra of R6G dyes catalyzed by UC@TiO<sub>2</sub>/Ag under full-spectrum Xe lamp. (B-D) The calculated time-dependent ratios of C/C<sub>0</sub>, first-order degradation rates, and reaction rate constants under full-spectrum Xe lamp in the absence or presence of different photocatalysts. (E) Time-dependent ratios of C/C<sub>0</sub> in the presence of different photocatalysts under UV-filtered Xe lamp. (F) Estimated contribution of non-UV irradiation (CNUV) in the degradation process of different photocatalysts.

Fig. 3C showed the kinetics of the photocatalytic reactions mentioned above, which can be described as pseudo first order by equation (1).

$$\ln \frac{C_t}{C_0} = -kt \quad (1)$$

The rate constants ( $k$ , min<sup>-1</sup>) were determined from plots of  $\ln(C/C_0)$  vs. irradiation time. The calculated rate constants with no photocatalysts, anatase, UC@TiO<sub>2</sub> and UC@TiO<sub>2</sub>/Ag are 0.0007, 0.0089, 0.0211 and 0.0282, respectively (Fig. 3D). The results indicated that the rate constant increased in the presence of UC cores. It can be concluded that the UC cores convert NIR light into UV light, since they can utilize both the UV and NIR lights simultaneously. The rate constant of UC@TiO<sub>2</sub>/Ag further increased might because the noble metal nanoparticles such as Ag and Au can enhance UC luminescence.<sup>34</sup>

Secondly, further experiments were carried out under irradiation of UV-filtered Xe lamp by the use of a UV filter with a wavelength cutoff of 420 nm in order to examine whether the non-UV irradiation can initiate the photocatalysis reaction on UC@TiO<sub>2</sub>/Ag (Fig. 3E). Similarly, almost no degradation of R6G occurred in the absence of photocatalysis, and understandably no obvious degradation occurred in the presence of anatase nanostructures. In contrast, the degradation ratios of R6G increased to about 35% and 40% after 4.5 h irradiation in the presence of UC@TiO<sub>2</sub> and UC@TiO<sub>2</sub>/Ag hybrid materials, respectively. Comparing the degradation ratios of R6G solution irradiated with Xe light source and UV-filtered Xe light source, we can estimate the contribution of non-UV irradiation in the

whole degradation process (Fig. 3F). The results revealed that non-UV irradiation did not contribute to the photocatalytic degradation of R6G dyes in the presence of only anatase nanostructures. However, once the UC cores existed, the contribution of non-UV in degrading R6G dyes with UC@TiO<sub>2</sub> and UC@TiO<sub>2</sub>/Ag hybrid materials reached to 30% and 35% after 2 h irradiation, respectively, implying a great improvement on utilization of simulated solar spectrum. Based on the results above, we can conclude that the contribution of non-UV light in the degradation process should mainly originate from the UC cores. The UC cores should act as the light converter to convert NIR light into UV light which can be efficiently absorbed by the TiO<sub>2</sub> comby shell and then initiate the photocatalytic reaction of the dye molecules, i.e. UC@TiO<sub>2</sub>/Ag hybrid materials can be used to activate TiO<sub>2</sub> and induces a relatively high photocatalytic activity under NIR irradiation.

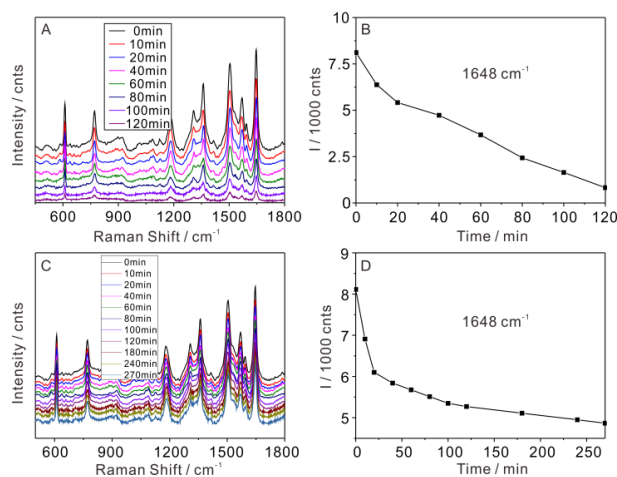


Fig. 4 (A, B) Time-course SERS spectra and time-dependent intensity at 1648 cm<sup>-1</sup> of R6G dyes catalyzed by UC@TiO<sub>2</sub>/Ag under full-spectrum Xe lamp. (C, D) Similar data resulted from the irradiation of UV-filtered Xe lamp.

As the complement of the experiments above, the remainder composites of each sample for UV-Vis absorbance measurement were also characterized by SERS experiments. Fig. 4A and B profiled the photocatalytic process of R6G dyes degraded by UC@TiO<sub>2</sub>/Ag hybrid materials under the irradiation of full-spectrum Xe lamp. As shown in Fig. 4A, the intense bands at 1361, 1503, 1570 and 1648 cm<sup>-1</sup> were assigned to carbon skeleton stretching modes, and the bands at 611, 771, 1181, and 1309 cm<sup>-1</sup> are assigned to C–C–C ring in-plane, out-of-plane bending, C–C stretching and C–O–C stretching vibrations, respectively. The whole spectral intensity of R6G gradually decreased with increasing irradiation times, and the intensity of one of the featured vibrations of R6G at 1648 cm<sup>-1</sup> was plotted as a function of the irradiation time (Fig. 4B). It is worth to notice that the main Raman vibrations of R6G can also be distinguished after 2 h irradiation in the presence of UC@TiO<sub>2</sub>/Ag hybrid materials. In contrast, the absorption peak of R6G at 520 nm could not be identified by UV-vis spectroscopy after 2 h in Fig. 3A. This comparison revealed the ultra-sensitivity features of SERS technique, highlighting the superiority of SERS compared to the traditional photocatalytic testing tools.

To clearly present the role of UC cores in light conversion, SERS

experiments under irradiation of UV-filtered Xe lamp were also carried out using the remainder composites catalyzed by UC@TiO<sub>2</sub>/Ag (Fig. 4C). It was found that the SERS intensity of R6G at 1648 cm<sup>-1</sup> also decreased gradually with increasing the irradiation time (Fig. 4D). According to the variation of SERS intensities in Fig. 4C and D, we also estimated that the contribution of non-UV irradiation in degrading R6G dyes with UC@TiO<sub>2</sub>/Ag hybrid materials, which reached to about 33% during the whole irradiation process of 2 h. It was consistent with the data, 35%, evaluated from the absorbance variation of UV-Vis spectroscopy in Fig. 3F. The results confirmed that UC cores can convert the NIR light into the UV light to activate TiO<sub>2</sub> and induce its photocatalytic activity under NIR irradiation.

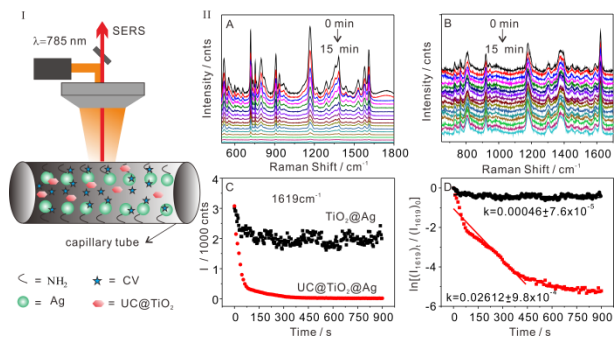


Fig. 5 (I) Schematic of SERS measurements under continuous exposure to a 785 nm laser on the capillary tube filled with the mixed solution of dyes and photocatalyst particles. (II) A and B, Time-dependent SERS mapping of CV dyes catalyzed by the UC@TiO<sub>2</sub>/Ag and TiO<sub>2</sub>/Ag; C, Time-dependent SERS intensities at 1619 cm<sup>-1</sup> band with the corresponding photocatalyst; and D, Determination of the reaction rate constants on UC@TiO<sub>2</sub>/Ag (red line) and TiO<sub>2</sub>/Ag (black line), respectively, according to Equation (2).

Both UV-Vis absorbance and SERS results above have evidenced that the presence of UC materials can initiate the non-UV photocatalytic of TiO<sub>2</sub>. However, the photocatalytic reaction kinetics under monochrome light source is more powerful proof for this new catalyst, UC@TiO<sub>2</sub>/Ag. Since SERS as a molecular surface-specific spectroscopic has been frequently applied in investigations of different types of reactions,<sup>35</sup> in-situ SERS experiments were designed under monochrome laser lines to directly monitor the catalytic reaction kinetics on UC@TiO<sub>2</sub>/Ag and solidly evidence the photocatalytic activity of TiO<sub>2</sub> under non-UV light (Fig. 5-I). To verify the universality of UC@TiO<sub>2</sub>/Ag, another resonant dye molecule CV, also a widely-used SERS reporter, was used to investigate the catalytic reaction kinetics. A certain amount of UC@TiO<sub>2</sub> was dispersed into 1 × 10<sup>-5</sup> M CV solution, the solution was then stirred for 12 h in dark, 15 μL of this solution was imported into the capillary tube decorated with Ag nanoparticles. A time-course SERS mapping was performed under continuous exposure to a 785 nm laser to examine the catalytic reaction kinetics of UC@TiO<sub>2</sub>/Ag (Fig. 5II-A). The Raman bands at 914, 805, and 726 cm<sup>-1</sup> C–N–C are symmetric stretch of the dimethylamino group, respectively. The in-plane aromatic C–H bending modes appear as a band at 1173 cm<sup>-1</sup> in the SERS spectrum. The spectra shows the intense peaks of the main CV vibrational features of carbon skeleton stretching modes at 1535, 1584 and 1619 cm<sup>-1</sup>. The Raman bands at 1352 and 1364 cm<sup>-1</sup> are symmetrical N–C–ring–C–C stretching mode, all

of them are due to CV vibration.<sup>36, 37</sup> As the exposure time increased, the SERS intensity of CV decreased dramatically, indicating the UC@TiO<sub>2</sub>/Ag related photocatalytic degradation of CV solution. The intensity of the typical CV bands at 1619 cm<sup>-1</sup> was plotted as a function of the exposure time (red line in Fig. 5II-C). As increasing irradiation time, the peak intensity became weaker and weaker and even disappeared at last, indicating the complete degradation of CV dye molecules. The results above clearly reveal the excellent photocatalytic capability of this UC@TiO<sub>2</sub>/Ag platform under the irradiation of monochrome laser line of 785 nm.

Nevertheless, apart from the photocatalysis effect in this SERS platform, the outrageous power of laser irradiation may induce many additional effects: photobleaching, photoinduced surface diffusion, substrate heating, or even possibly substrate morphology changes, which should cause the SERS signals decay.<sup>38</sup> As a control, a similar SERS experiment was also carried out on the TiO<sub>2</sub>/Ag nanostructures without the UC cores under the same excitation of 785 nm laser to corroborate the role of UC cores in the light conversion. Only small changes in SERS spectra of CV were observed as illustrated by the time-course SERS mapping data (Fig. 5II-B). The fingerprint information of CV almost had no changes after 15 minutes, and the intensity of the typical CV bands at 1619 cm<sup>-1</sup> only had a little decreased in the first 30s and then kept stable in later times (black line in Fig. 5II-C). Hence, the chosen laser power in our SERS experiments was appropriate and did not induce obvious signals decay except the photocatalysis effect. This result further confirmed that the CV dye molecules cannot be degraded effectively by only TiO<sub>2</sub>/Ag under the same excitation of 785 nm lasers, i.e. the sole TiO<sub>2</sub> cannot efficiently absorb NIR light to realize the photocatalysis of CV because of its large band gap (ca. 3.2 eV).

In order to determine the rate constants of the photocatalytic reaction on UC@TiO<sub>2</sub>/Ag hybrid materials under NIR irradiation, the intensity of the 1619 cm<sup>-1</sup> band as a function of exposure time was normalized by the intensity at time ZERO, and the logarithm of the ratio of relative intensities was plotted as a function of irradiation time in Fig. 5II-D. The reaction rate constant, *k*, of the pseudo-first-order kinetics reaction can be determined by Equation (2).<sup>35</sup>

$$-kt = \ln \frac{[CV]_t}{[CV]_0} = \ln \frac{I_t}{I_0} \quad (2)$$

where [CV]<sub>t</sub> and [CV]<sub>0</sub> is the number of adsorbed CV molecules on the SERS substrate at time *t* and ZERO, respectively, and I<sub>t</sub> and I<sub>0</sub> is the intensity of the 1619 cm<sup>-1</sup> band at time *t* and ZERO, respectively. The calculated reaction rate constants are 0.02612 s<sup>-1</sup> for UC@TiO<sub>2</sub>/Ag (red line in Fig. 5II-D) and 0.00046 s<sup>-1</sup> for TiO<sub>2</sub>/Ag (black line in Fig. 5II-D), the difference of these two numbers is nearly 58 times, indicating that the UC cores significantly initiate and amplify the photocatalytic activity of TiO<sub>2</sub>/Ag under NIR excitation. UC@TiO<sub>2</sub>/Ag hybrid materials can be used to activate TiO<sub>2</sub> and induces a relatively high photocatalytic activity under NIR irradiation.

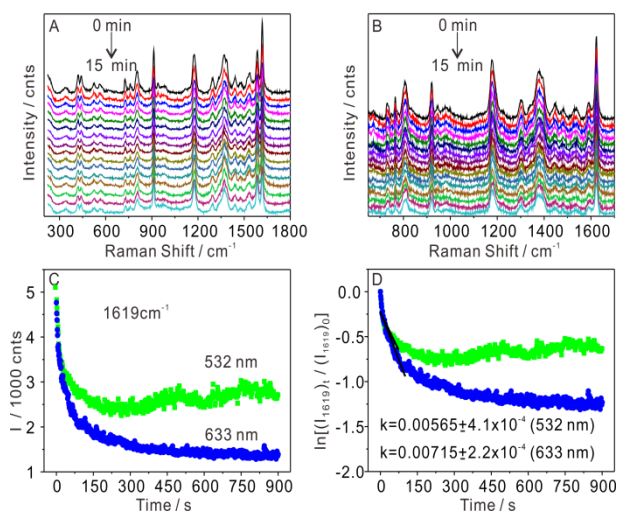


Fig. 6 (A and B) Time-dependent SERS mapping of CV dyes photo-catalyzed by UC@TiO<sub>2</sub>/Ag under continuous exposure to 532 nm and 633 nm laser, respectively. (C) Time-dependent SERS intensities of 1619 cm<sup>-1</sup> band under exposure of the corresponding laser. (D) Determination of the reaction rate constants according to Equation (2), green line for 532 nm laser and blue line for 633 nm laser, respectively.

It's worth pointing out that the nano-structural TiO<sub>2</sub> comby shell coated on UC microcrystals must has some different aspects from solely prepared TiO<sub>2</sub> nanostructures, which may cause some controversy on the horizontal comparison above. As the longitudinal comparison of a same sample, UC@TiO<sub>2</sub>/Ag, another two different monochrome laser lines (532 nm and 633 nm) were employed to carry out time-mapping SERS experiments (Fig. 6), which further demonstrates the key role of UC cores in the NIR responsive photocatalysis of TiO<sub>2</sub> under monochrome laser. Similar time-course SERS mappings of the catalytic reaction kinetics of UC@TiO<sub>2</sub>/Ag were performed under continuous exposure to the 532 nm laser (Fig. 6A) and 633 nm laser (Fig. 6B), respectively. As increasing the irradiation time, all the peak intensities became weaker at the beginning under two different lasers, and then the peak intensities of the spectra became stable, indicating a balance of the residual number of adsorbed CV molecules on the SERS substrate. The UC cannot efficiently convert the lasers of 532 nm and 633 nm into UV light to realize further photocatalytic degradation. The intensity of the typical CV bands at 1619 cm<sup>-1</sup> had a little decreased in the first 60s under continuous exposure to a 532 nm laser, and then the intensity kept stable as the time increased (green line in Fig. 6C). Similarly, a little decreased of the intensity at 1619 cm<sup>-1</sup> was observed in the first 80s under continuous exposure to a 633 nm laser, and then the intensity kept stable as the time increased (blue line in Fig. 6C). Fig. 6C clearly revealed that the final intensity at 1619 cm<sup>-1</sup> under 633 nm laser was weaker than that under 532 nm laser. We estimated the reaction rate constants for UC@TiO<sub>2</sub>/Ag under 532 nm laser ( $k=0.00565\text{ s}^{-1}$ , green line in Fig. 6D) and 633 nm laser ( $k=0.00715\text{ s}^{-1}$ , green line in Fig. 6D) by the Equation (2). The data showed that the reaction rate constant under 633 nm laser was a little bit larger than that under 532 nm laser, but both of them were much smaller than that under the 785 nm laser. The reaction rate constant sharply decreased with shorter wavelengths, indicating a wavelength-dependent behavior of photocatalysis.

The reaction rate constants of these three monochrome lasers were consistent with the conclusion that UC materials can be better activated by longer wavelength irradiation. It was also evidenced from another side that the UC materials played the key role in the photocatalytic degradation with UC@TiO<sub>2</sub>/Ag under the NIR excitation.

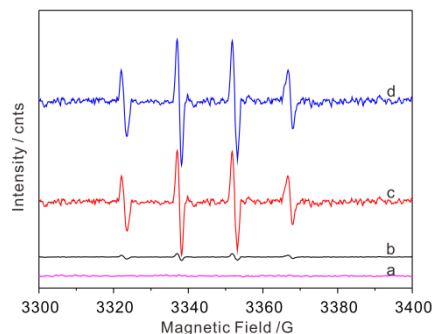
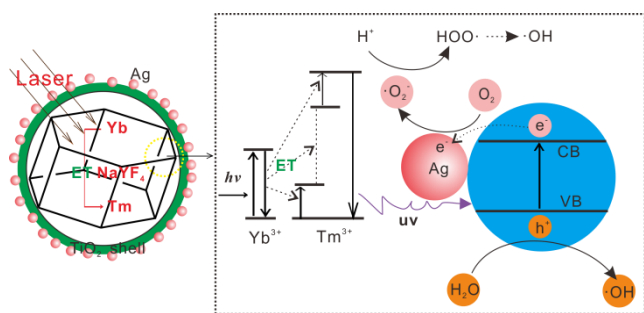


Fig. 7 ESR spectral features of the DMPO-OH spin adducts in the system without addition CV or R6G under irradiation of full-spectrum Xe lamp with different photocatalysts (a-d) water alone, pure TiO<sub>2</sub> anatase, UC@TiO<sub>2</sub> and UC@TiO<sub>2</sub>/Ag, respectively.

Meanwhile the ESR method, widely used in the processes of photogenerated charge transfer, also revealed the key role of UC materials in the photocatalytic degradation by the ESR spectra of ·OH radical.<sup>39, 40</sup> ESR spectra of DMPO spin adducts were recorded following the same conditions as used in the photocatalytic degradation of R6G. ESR spectral features of the DMPO-OH spin adducts in the system without addition CV or R6G under irradiation of full-spectrum Xe lamp with different photocatalysts (a-d) water alone, pure TiO<sub>2</sub> anatase and UC@TiO<sub>2</sub> and UC@TiO<sub>2</sub>/Ag were shown in Fig. 7. After the same irradiation time, line a has no signal, lines b-d displaying signals with characteristic intensity 1:2:2:1 for DMPO-OH adducts was obtained without addition CV or R6G to the photocatalytic system, which indicated that the ·OH radical was surely formed under the present conditions.<sup>41</sup> It revealed that UC can convert NIR into UV to realize the photocatalysis of broadband TiO<sub>2</sub>. It also can be seen that the intensities of signal strengthened increased in the presence of UC materials, indicating the concentrations of free radicals increased. The major reason of this phenomenon was that crystallized TiO<sub>2</sub> comby shell can efficiently absorb UV lights (~350 nm) emitted from UC cores upon Xe lamp irradiation. The presence of noble metal Ag nanoparticles can enhance UC luminescence to form the stronger UV emission, so the intensity of line d is 1.2 fold than that of than line c. This phenomenon was consistent with the result of the photocatalytic degradation and it also revealed the key role of UC materials in photocatalytic degradation with UC@TiO<sub>2</sub>/Ag under non-UV excitation.



Scheme 2 Illustrated mechanism of NIR-activated photocatalysis on UC@TiO<sub>2</sub>/Ag.

Nanoscience is developing fast, and this is particularly true for the coupling of photocatalytic materials and upconversion structures. Few examples of well-defined UC materials-initiated non-UV photocatalytic enhancement have been reported. In closing, it is worth speculating on the origin of excellent non-UV photocatalytic capability in UC@TiO<sub>2</sub>/Ag structures (Scheme 2). As evidenced by UV-Vis, SERS and ESR data, the Yb<sup>3+</sup> ions act as sensitizers and are the primary absorbers of the NIR excitation, and then three successive energy transfers from Yb<sup>3+</sup> to Tm<sup>3+</sup> populate the <sup>3</sup>H<sub>5</sub>, <sup>3</sup>F<sub>2</sub>, and <sup>1</sup>G<sub>4</sub> levels. At last, <sup>1</sup>D<sub>2</sub>→<sup>3</sup>F<sub>4</sub>, <sup>1</sup>G<sub>4</sub>→<sup>3</sup>H<sub>6</sub>, <sup>3</sup>P<sub>0</sub>→<sup>3</sup>F<sub>4</sub> and <sup>1</sup>D<sub>2</sub>→<sup>3</sup>H<sub>6</sub> transitions produce the blue emissions at 450 nm, 474 nm, and UV emissions at 349 nm, 362nm, respectively. Here the <sup>3</sup>P<sub>0</sub> and <sup>1</sup>D<sub>2</sub> levels are the predominant excited state in this material as suggested by the strongest UV emission.<sup>33</sup> The presence of noble metal Ag NPs can enhance UC luminescence to form the stronger UV emission. Moreover, Ag NPs can use as co-catalyst to further improved the photocatalytic performance. When TiO<sub>2</sub> is activated by UV light can produce electrons and holes in the conduction band and the valence band. Because the Fermi level of TiO<sub>2</sub> is higher than that of Ag, the photo-generated electrons of TiO<sub>2</sub> can be transferred to Ag.<sup>42</sup> Then the electrons are scavenged by molecular oxygen to form superoxide ·O<sub>2</sub><sup>-</sup> radical anions, while holes can react with H<sub>2</sub>O to form hydroxyl radicals (·OH).<sup>4</sup> Therefore, the organic molecules present in the solution will then react with these oxidizing agents to induce oxidative degradation. The electrons transfer from TiO<sub>2</sub> to Ag NPs will effectively inhibit the recombination of the excited electrons and holes, and therefore increase the photocatalytic performance of the NaYF<sub>4</sub>:Yb,Tm@TiO<sub>2</sub>/Ag Core@Comby Shell Nanostructures.

## Conclusions

In summary, a novel non-UV photocatalyst, the UC@TiO<sub>2</sub>/Ag composite were prepared by a simple and efficient method, which was further incorporated into SERS-active substrates. Both the UV-filtered Xe lamp and monochrome laser lines on SERS apparatus were used to investigate the photocatalytic activities of this core@comby shell nanocomposites, and the catalytic reaction kinetics were successfully monitored by SERS technique. SERS analysis by virtue of monochrome laser lines, for the first time, provided the direct evidence to prove the capability of UC-initiated non-UV photocatalysis and the improvement of the utilization of non-UV lights on TiO<sub>2</sub>. The composite exhibits excellent photocatalytic activity as the UC cores can efficiently

convert NIR light into UV light. This new system can efficiently utilize different bands of the solar spectrum and greatly improve the utilization range of solar energy, which enabling a promising application in emerging solar-energy technologies. In addition, it also provides a new chance for the applications of SERS technique, as well as a new strategy to research the photocatalytic degradation of environmental pollutants.

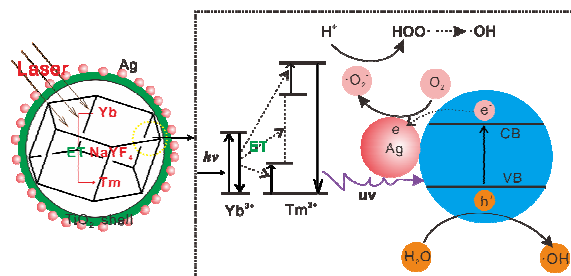
## Acknowledgment

This work was supported by the National Basic Research Program of China (2011CB933700), the National Instrumentation Program of China (2011YQ0301241001 & 2011YQ0301241101), National Natural Science Foundation of China (21305142), and Natural Science Foundation of Anhui Province, China (1308085QB27). A special thank is given to Dr. Wei Tong, Youming Zou and Lu Yu from High Magnetic Field Laboratory (Chinese Academy of Sciences, Hefei 230031, China) for support in ESR measurements and discussion.

## Notes and references

- Institute of Intelligent Machines, Chinese Academy of Sciences, Hefei 230031, China.*  
Phone: +86-551-6559-2385. Fax: +86-551-6559-2420. E-mail: hlliu@iim.ac.cn, lbyang@iim.ac.cn.
- † Electronic Supplementary Information (ESI) available: [SEM, TEM and EDX]. See DOI: 10.1039/b000000x/
- S. Furukawa, T. Shishido, K. Teramura and T. Tanaka, *Acs Catal.*, 2012, 2, 175-179.
  - E. Grabowska, M. Diak, M. Marchelek and A. Zaleska, *Appl. Catal. B-Environ.*, 2014, 156, 213-235.
  - R. Asahi, Y. Taga, W. Mannstadt and A. J. Freeman, *Phys. Rev. B*, 2000, 61, 7459-7465.
  - Y. N. Tang, W. H. Di, X. S. Zhai, R. Y. Yang and W. P. Qin, *Acs Catal.*, 2013, 3, 405-412.
  - Y. Shiraishi, H. Sakamoto, K. Fujiwara, S. Ichikawa and T. Hirai, *Acs Catal.*, 2014, 4, 2418-2425.
  - J. Zhang, L. S. Qian, W. Fu, J. H. Xi and Z. G. Ji, *J. Am. Ceram. Soc.*, 2014, 97, 2615-2622.
  - K. Vignesh, M. Rajarajan and A. Suganthi, *J. Ind. Eng. Chem.*, 2014, 20, 3826-3833.
  - Z. G. Xiong and X. S. Zhao, *J. Am. Chem. Soc.*, 2012, 134, 5754-5757.
  - D. Tsukamoto, Y. Shiraishi, Y. Sugano, S. Ichikawa, S. Tanaka and T. Hirai, *J. Am. Chem. Soc.*, 2012, 134, 6309-6315.
  - A. Primo, T. Marino, A. Corma, R. Molinari and H. Garcia, *J. Am. Chem. Soc.*, 2012, 134, 1892-1892.
  - M. Zhang, Q. Wang, C. C. Chen, L. Zang, W. H. Ma and J. C. Zhao, *Angew. Chem.Int. Edit.*, 2009, 48, 6081-6084.
  - J. L. Hu, H. S. Qian, J. J. Li, Y. Hu, Z. Q. Li and S. H. Yu, *Part. Part. Syst. Char.*, 2013, 30, 306-310.
  - L. Xu, E. M. P. Steinmiller and S. E. Skrabalak, *J. Phys. Chem. C*, 2012, 116, 871-877.
  - H. Y. Chuang and D. H. Chen, *Nanotechnology*, 2009, 20, 105704-105713.
  - J. Bai, J. H. Li, Y. B. Liu, B. X. Zhou and W. M. Cai, *Appl. Catal. B-Environ.*, 2010, 95, 408-413.
  - S. J. Zhuo, M. W. Shao and S. T. Lee, *ACS NANO*, 2012, 6, 1059-1064.
  - H. Q. Wang, M. Batentschuk, A. Osvet, L. Pinna and C. J. Brabec, *Adv. Mater.*, 2011, 23, 2675-2680.
  - W. Xu, X. Bai, S. Xu, Y. S. Zhu, L. Xia and H. W. Song, *Rsc Adv.*, 2012, 2, 2047-2054.
  - F. Wang, D. Banerjee, Y. S. Liu, X. Y. Chen and X. G. Liu, *Analyst*, 2010, 135, 1839-1854.

20. F. Wang, Y. Han, C. S. Lim, Y. H. Lu, J. Wang, J. Xu, H. Y. Chen, C. Zhang, M. H. Hong and X. G. Liu, *Nature*, 2010, 463, 1061-1065.
21. W. P. Qin, D. S. Zhang, D. Zhao, L. L. Wang and K. Z. Zheng, *Chem. Commun.*, 2010, 46, 2304-2306.
22. Z. Q. Li, C. L. Li, Y. Y. Mei, L. M. Wang, G. H. Du and Y. J. Xiong, *Nanoscale*, 2013, 5, 3030-3036.
23. H. L. Liu, Z. L. Yang, L. Y. Meng, Y. D. Sun, J. Wang, L. B. Yang, J. H. Liu and Z. Q. Tian, *J. Am. Chem. Soc.*, 2014, 136, 5332-5341.
24. Y. M. Ma, H. L. Liu, K. Qian, L. B. Yang and J. H. Liu, *J. Colloid Interf. Sci.*, 2012, 386, 451-455.
25. H. L. Liu, D. Y. Lin, Y. D. Sun, L. B. Yang and J. H. Liu, *Chem.-Eur. J.*, 2013, 19, 8789-8796.
26. A. McLintock, C. A. Cunha-Matos, M. Zagnoni, O. R. Millington and A. W. Wark, *ACS NANO*, 2014, 8, 8600-8609.
27. H. B. Yao, L. B. Mao, Y. X. Yan, H. P. Cong, X. Lei and S. H. Yu, *ACS NANO*, 2012, 6, 8250-8260.
28. Y. Wu, X. Shen, S. X. Dai, Y. S. Xu, F. F. Chen, C. G. Lin, T. F. Xu and Q. H. Nie, *J. Phys. Chem. C*, 2011, 115, 25040-25045.
29. J. C. Goldschmidt, S. Fischer, H. Steinkemper, F. Hallermann, G. von Plessen, K. W. Kramer, D. Biner and M. Hermle, *Ieee J. Photovolt.*, 2012, 2, 134-140.
30. Z. Q. Li, S. Chen, J. J. Li, Q. Q. Liu, Z. Sun, Z. B. Wang and S. M. Huang, *J. Appl. Phys.*, 2012, 111.
31. Y. M. Ma, Q. Q. Ding, L. B. Yang, L. Zhang and Y. H. Shen, *Appl. Surf. Sci.*, 2013, 265, 346-351.
32. Y. J. Sun, Y. Chen, L. J. Tian, Y. Yu, X. G. Kong, J. W. Zhao and H. Zhang, *Nanotechnology*, 2007, 18.
33. X. R. Zhang, Y. Li, H. R. Su and S. S. Zhang, *Biosens. Bioelectron.*, 2010, 25, 1338-1343.
34. N. Liu, W. P. Qin, G. S. Qin, T. Jiang and D. Zhao, *Chem. Commun.*, 2011, 47, 7671-7673.
35. V. Joseph, C. Engelbrekt, J. D. Zhang, U. Gernert, J. Ulstrup and J. Kneipp, *Angew. Chem. Int. Edit.*, 2012, 51, 7592-7596.
36. M. Volny, A. Sengupta, C. B. Wilson, B. D. Swanson, E. J. Davis and F. Turecek, *Anal. Chem.*, 2007, 79, 4543-4551.
37. Y. J. Ye, J. Chen, Q. Q. Ding, D. Y. Lin, R. L. Dong, L. B. Yang and J. H. Liu, *Nanoscale*, 2013, 5, 5887-5895.
38. H. Liu, Y. Sun, Z. Jin, L. Yang and J. Liu, *Chem. Sci.*, 2013, 4, 3490-3496.
39. P. Luan, M. Z. Xie, D. N. Liu, X. D. Fu and L. Q. Jing, *Sci. Rep-Uk*, 2014, 4.
40. Z. Tzitrinovich, A. Lipovsky, A. Gedanken and R. Lubart, *Phys. Chem. Chem. Phys.*, 2013, 15, 12977-12981.
41. J. Yang, J. Dai, C. C. Chen and J. C. Zhao, *J. Photoch. Photobio. A*, 2009, 208, 66-77.
42. Y. Zhou, J. Chen, L. Zhang and L. B. Yang, *Eur. J. Inorg. Chem.*, 2012, 3176-3182.



Enhanced photocatalysis of  $\text{NaYF}_4:\text{Yb,Tm}@\text{TiO}_2/\text{Ag}$  under non-ultraviolet was demonstrated by monitoring the photocatalytic kinetics with SERS technique.